RSC Advances

ROYAL SOCIETY OF CHEMISTRY

www.rsc.org/advances

Organic-Inorganic Hybrid $CH_3NH_3PbI_3$ Perovskite Materials as Channels in Thin-Film Field-Effect Transistors

Yuxiang Wu, Juan Li*, Jian Xu, Yangyang Du, Like Huang, Jian Ni, Hongkun Cai, Jianjun Zhang

Institute of Photo-Electronics, Nankai University, The Tianjin Key Laboratory for Optical-Electronic Thin Film Devices and Technology, Tianjin 300071, China

ABSTRACT:

Organic-inorganic hybrid perovskite materials promise both the superior carrier mobility of inorganic semiconductors and the processability of organic materials which make organic-inorganic hybrid perovskite materials good substitutes in all the applications put forth for organic materials and extend their application to higher speed devices than is presently possible with either a-Si or organic semiconductors. Recent reports have shown high carrier mobility and long electron-hole diffusion lengths of organic-inorganic hybrid perovskite materials. [1] So we demonstrated a thin-film field-effect transistor having an organic-inorganic hybrid $CH_3NH_3PbI_3$ material as the semiconducting channel based on these advantages via low-temperature vapor-assisted solution process. The obvious electrical field effect is obtained in organic-inorganic hybrid $CH_3NH_3PbI_3$ perovskite TFTs with field-effect mobility of 396.2 cm^2/V.s, current modulation greater than 10^4, sub-threshold current of 0.4035 V/decade and threshold voltage of -3.501 V.

KEYWORDS: thin-film field-effect transistor; organic-inorganic hybrid $CH_3NH_3PbI_3$; low-temperature vapor-assisted solution process.

*Corresponding author: lj1018@nankai.edu.cn (J. Li)

Tel: +8613302138508

1. Introduction

In recent years, display devices have become common due to the development of mobiles phones, flat-screen TVs, personal computer monitors, etc. The essential element for such devices is a thin-film transistor (TFT).

TFTs are usually manufactured using organic materials or inorganic materials as channels. Organic thin-film transistors (OTFTs) offer many advantages such as processability and mechanical flexibility over inorganic technologies [2-4] and have been developed for use in a wide range of applications including displays [5,6], sensors [7,8], and radio frequency identification [9,10]. However, mobilities of organic TFTs are usually lower than 1 cm^2/V.s. Athough many methods have been developed to enhance mobilities of organic TFTs，most mobilities reported for organic TFTs are lower than 10cm^2/V.s[11]. The weak van der Waals interaction bonding neighboring molecules limits their carrier mobility to further improve. Therefore, the low carrier mobility of organic TFTs limits their device-switching speeds and their range of potential applications.

As to the inorganic TFTs, the polycrystalline silicon (poly-Si) (50~400 cm^2/Vs) TFT has a mobility one or two magnitudes higher than that of the amorphous silicon (a-Si:H) TFT (1 cm^2/Vs)and organic TFT. However, the fabrication of this material is complicated and needs a temperature higher than 500℃(even up to 900℃) for crystallization，which is not suitable for flexible electronics application. Alternative semiconducting materials for thin field-effect transistors (TFTs), which have mobility at least comparable to that of amorphous silicon (a-Si) and may also be easily processed with low-cost techniques, are required to enable new opportunities for display and storage technologies.

Recently, the amorphous metal-oxide show many advantageous properties, such as the high mobility, optical transparency, and low process temperature. However, mobilities of these

TFTs are usually lower than 10cm^2/V.s. In order to achieve a high mobility, it has to be annealed at a temperature higher than about 300℃, which is a hurdle for the plastic film substrate[12-19]. Advanced materials and processing techniques developed in recent years, such as nanowires, single-walled carbon nanotubes (SWCNTs) and grapheme, which have been fabricated into TFTs for flexible electronic applications. These methods usually need complicated process procedures or high temperatures [19-24] even if the device performance could be enhanced. Despite great efforts being exerted in this field, so far no one has succeeded in demonstrating a good performance TFT with relatively simple and real low-temperature processing suitable for high quality, low-cost and flexible displays.

In the present work, we have proposed a novel TFT that has an organic-inorganic hybrid perovskite as channel layer. This material is crystallized from organic halide and metal halide salts to form crystals in the ABX_3 structure, where A is the organic cation, B is the metal cation and X is the halide anion (see Fig. 1).The inorganic component forms an extended framework bound by strong covalent or ionic (or both) interactions to provide high carrier mobility. The organic component facilitates the self-assembly of these materials, enabling hybrids to be deposited by the same simple, low-cost, low-temperature processes as the organic materials. The organic component is also used to tailor the electronic properties of the inorganic framework. Engineering the organic-inorganic hybrid perovskite on the molecular scale may be done to maximize carrier mobility. The combination of high carrier mobility and ease of processing may make organic-inorganic hybrid perovskite materials good substitutes in all the applications put forth for organic materials. The potentially higher carrier mobility of organic-inorganic hybrid perovskite materials may extend their application to higher speed devices than is presently possible with

either a-Si or organic semiconductors. As we know, the organic–inorganic hybrid perovskite materials have been successfully used in solar cells[25-27], which the power conversion efficiency (PCE) has been up to 20.1%[28] from 3.8%[29] due to distinct merits of organic–inorganic hybrid perovskite materials [1,29-32]. Thus the remarkable properties of organic–inorganic hybrid perovskite materials illustrate that they are suitable for the application in TFTs.

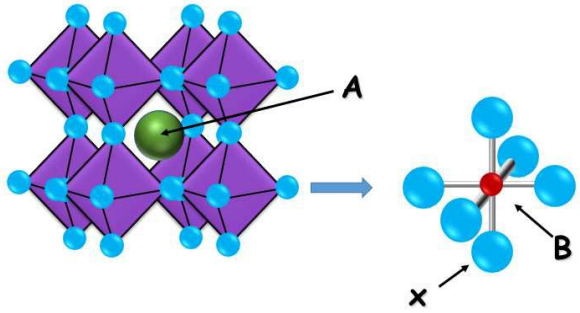

Fig. 1 Perovskite ABX_3 crystal structure where typically A = CH3NH3$^+$, B = Pb^{2+} and X = I^-, Br^-, Cl^-, or mixtures thereof.

In this paper, we proposed a new kind of thin-film field-effect transistor using organic-inorganic hybrid perovskite $CH_3NH_3PbI_3$ material as the semiconducting channel.

2. Experimental section

2.1. Thin film fabrication

Here, we used a facile vapor assisted solution approach to perovskite material formations with enhanced controllability over the film quality [33], where the inorganic framework film was formed by depositing precursor solution on the substrates, and subsequently treated with the desired organic vapor (Fig. 2). PbI_2 solution was prepared in DMF at the concentration of 345 mg/ml. The prepared PbI_2 solution was preheated at 110 °C on a hot plate, followed by spin coating on the substrates at 4000 rpm for 40 s, at the same time a dry nitrogen gas flow was blown over the surface of the PbI_2 solution during the spin-coating process in air [26], then put back on the hot plate for 15 min of drying. To obtain the perovskite thin film, substrates with PbI_2 film were

then put into a vacuum coating machine, then CH_3NH_3I was deposited by thermal evaporation for 0.5 h. After cooling down to room temperature, the perovskite films was annealed for 0.3 h at 100°C.

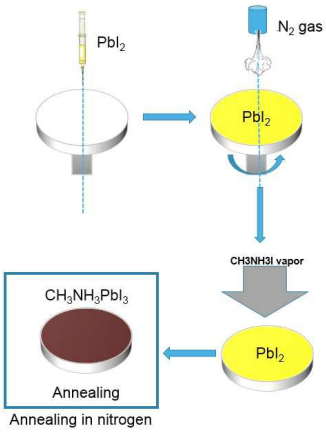

Fig. 2 Schematic illustration of the procedure of perovskite thin film prepared via modified vapor-assisted solution process.

2.2. Thin film field-effect transistors (TFTs) fabrication

Fig. 3 shows the structure of device of our perovskite thin film field-effect transistors. [34] Heavily n-doped silicon wafers were used as the gate electrode. The gate dielectric layer was a 200nm thermally grown silicon dioxide. Organic-inorganic hybrid $CH_3NH_3PbI_3$ as the semiconducting channel was obtained via modified vapor-assisted solution process. High work-function metal source and drain electrodes such as Ag were deposited by evaporation through a shadow mask.

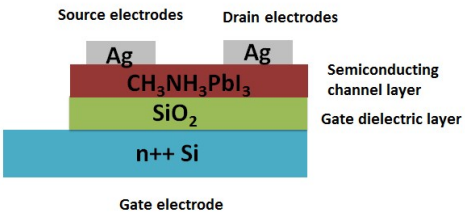

Fig. 3 Device architecture. Schematic view of the perovskite TFT configuration: n++ Si substrate, SiO_2 gate insulator, $CH_3NH_3PbI_3$ film as the semiconducting channel, Ag source and drain electrodes.

2.3. Analysis of characterizations on active layers and analysis of TFT devices

The crystal structures of the $CH_3NH_3PbI_3$ films were characterized by X-ray diffraction (XRD, Philips PANalytical X'Pert Pro) with a copper x-ray source, and the surface morphologies were observed by scanning electron microscope (SEM, Hitachi SU8010) and atomic force microscopy (AFM) (Seiko SPA-400SPM UNIT). The photoluminescence (PL) spectrum measurements were conducted by a Fluorolog-3-212 steady state spectrometer. The laser wavelength is 350nm. The electrical performance of the TFT devices was measured with Keysight Technologies B1500A Semiconductor Device Analyzer. All devices were tested in air and at room temperature. Device performances were extracted by the standard field-effect transistor equations that apply to both organic and inorganic TFTs. The mobility of the device was extracted using the following equation:

$$\mu = (dI_{DS}/dV_G)\ (L/V_D C_i W)$$

Where μ is the device mobility, I_D and V_G respectively correspond to the drain current and gate voltage, L channel length, W channel width and C_i the gate insulator capacitance. The sub-threshold slope (S.S.) was calculated as the minimum value of the inverse slope of the $\log I_D$ versus V_G:

$$SS = (dV_G/d\log I_{DS})$$

3. Results and discussion

Organic-inorganic hybrid $CH_3NH_3PbI_3$ perovskite materials via modified vapor-assisted solution process were obtained with full surface coverage, uniform grain structure with grain size up to micrometers. The key step is film growth via in situ reaction of the as-deposited film of PbI_2 with CH_3NH_3I vapor (Fig. 2). This method is conceptually different from the current solution process and vacuum deposition by avoiding co-deposition of organic and inorganic species. In one-step deposition, the two precursor salts (metal halide and organic halide) are dissolved in an

organic solvent, the mixture is spin-coated onto a substrate, and the perovskite is formed through an annealing process at around 100℃,finally the perovskite crystals are micrometer-sized in size. However spin-coating the mixture directly onto a substrate initially resulted in a dewetting effect,[35] thus leading to poor surface coverage.[36, 37] As to the co-deposition technique [38], although nearly 100% surface coverage can be obtained, the perovskite crystals obtained are a few hundred nanometers in size, and thus smaller than the micrometer-sized platelets obtained from spin-coating. However the modified vapor-assisted solution process we used to fabricate perovskite films combine the full surface coverage with micrometer-sized crystals, which indicates high-quality films.

Meanwhile, an additional step was introduced where a dry nitrogen gas flow was blown over the surface of the PbI_2, promoting evaporation of the solvent and accelerating the supersaturation of the solution. In general, a solution precipitation process involves two steps: nucleation and crystal growth. Nuclei will form when a solution reaches supersaturation and the volume of the nuclei in the system would depend on the rate of nucleation and the degree of the supersaturation. This addition step where a dry nitrogen gas flow was blown over the surface facilitated a high degree of supersaturation of the PbI_2 in the wet film during spin-coating, resulting in a large number of nuclei which reacted with CH_3NH_3I vapor and, finally, the full coverage of the $CH_3NH_3PbI_3$ layer was obtained when the as-deposited film of PbI_2 completely reacted with CH_3NH_3I vapor. This process takes advantage of the kinetic reactivity of CH_3NH_3I and thermodynamic stability of perovskite during the growth process in situ and provides films with grain sizes up to microscale, full surface coverage, and small surface roughness, which is required for TFTs channel.

Firstly, to optimize the perovskite films, we researched the influence of PbI_2 solution concentration and the amount of evaporated CH_3NH_3I on perovskite films performance, respectively.

3.1 The influence of PbI_2 solution concentration on perovskite films performance

Figure 4 shows the top-view SEM images of PbI_2 layer and perovskite films prepared with different PbI_2 solution concentration varied from 100mg/ml to 500mg/ml, where the amount of CH_3NH_3I is 159mg. And X-ray diffraction (XRD) measurements of perovskite films corresponding to different PbI_2 solution concentration were taken. As shown in Fig. 4F, a set of strong peaks at 14.08°, 28.41° and 31.85°, assigned to (110), (220) and (310) of the $CH_3NH_3PbI_3$ crystal, [33,35] indicate an orthorhombic crystal structure of halide perovskite with high crystallinity. Meanwhile a tiny signature peak at 12.65° is observed in Fig. 4F (c,d), [36] which indicates a low-level impurity of PbI_2. Table 1 shows the surface roughness of PbI_2 layer and perovskite films with different PbI_2 solution concentration. We have found that the PbI_2 solution concentration has main influence on the roughness and the PbI_2 residue of perovskite films rather than the grain size. As can been seen, with the PbI_2 solution concentration increasing, the surface roughness of the PbI_2 film gradually increases (see Table 1). This change benefit PbI_2 to contact MAI and convert completely to perovskite, where final perovskite films are obtained without PbI_2 residue as shown in Fig. 4F (d,e). At the same time, the sufficient reaction is also beneficial to reducing surface roughness of perovskite films, as shown in Fig. 4 and Table 1. However，when the PbI_2 solution concentration is too high, for instance, 500mg/ml, the surface roughness of PbI_2 layer would increase, leading to the increase of the surface roughness of the resulted perovskite films. Hence，considering with the surface roughness of perovskite films and the PbI_2

residue.，we suggest that the PbI_2 solution concentration of 345mg/ml is suitable to fabricate perovskite films.

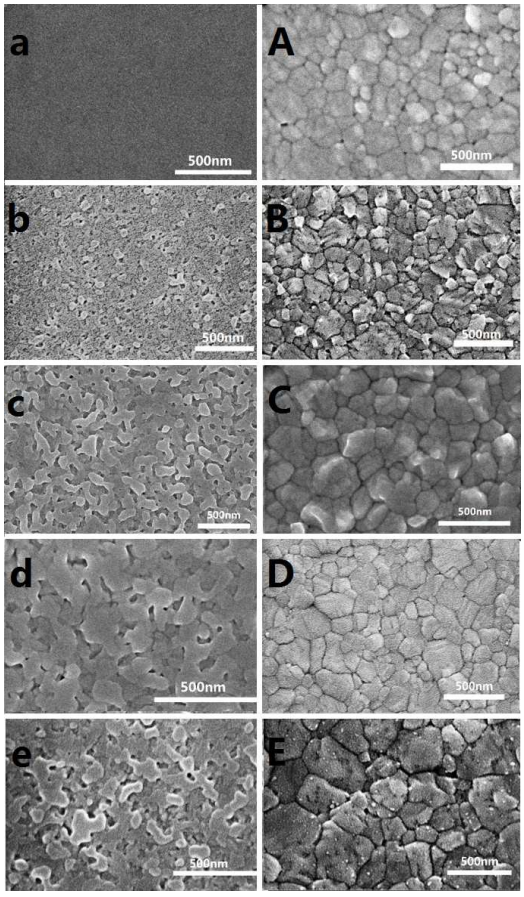

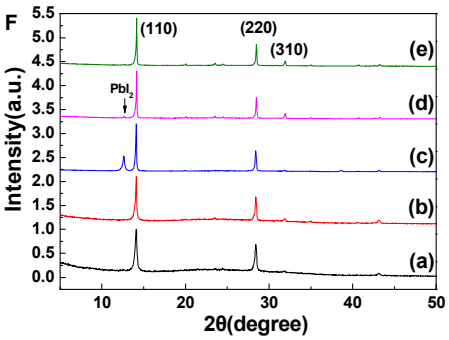

Fig. 4 SEM top-view images of PbI_2-coated films (a~e) and $CH_3NH_3PbI_3$ films (A~E): PbI2 solution concentration varied from 100mg/ml(a,A), 250mg/ml(b,B), 285mg/ml(c,C), 345mg/ml(d,D), 500mg/ml(e,E); (F) X-ray diffraction pattern of $CH_3NH_3PbI_3$ films: PbI_2 solution concentration varied from 100mg/ml(a), 250mg/ml(b), 285mg/ml(c), 345mg/ml (d), to 500mg/ml(e).

Table 1 Parameters derived from AFM measurements corresponding to Fig. 4a~4E

Roughness surface RMS (nm)	**100mg/ml**	**250mg/ml**	**285mg/ml**	**345mg/ml**	**500mg/ml**
PbI_2 films	7.184E-01	2.029E+00	1.255E+00	1.852E+00	6.035E+00
$CH_3NH_3PbI_3$ films	1.352E+01	1.460E+01	1.128E+01	1.948E+00	1.083E+01

3.2 The influence of amount of CH3NH3I evaporation on perovskite films performance

In order to further optimize $CH_3NH_3PbI_3$ films to obtain larger crystals, we prepared three types of $CH_3NH_3PbI_3$ thin films: Type A, the amount of CH_3NH_3I precursor used in thermal evaporation process was 120mg; Type B, the amount of CH_3NH_3I precursor used in thermal

evaporation process was 200mg; Type C, the amount of CH_3NH_3I precursor used in thermal evaporation process was 280mg. Fig. 5 present scanning electron microscope (SEM) images of $CH_3NH_3PbI_3$ films interfaced to SiO_2 substrate.

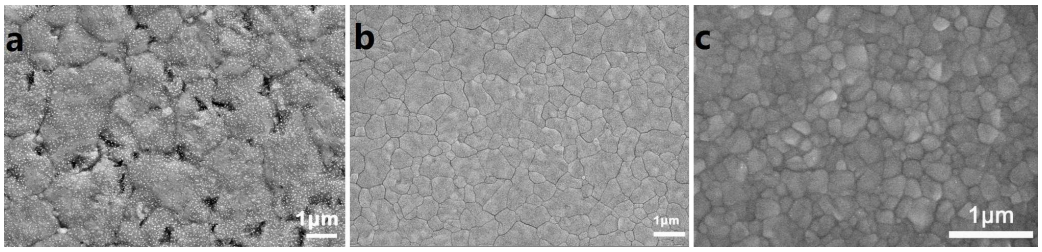

Fig. 5 Scanning electron microscopy (SEM) images of the $CH_3NH_3PbI_3$ film: the amount of CH_3NH_3I precursor in thermal evaporation process is 120mg (a), 200mg (b), 280mg (c), respectively.

For type A (Fig. 5a), the grain size is the biggest, but there are many voids among adjacent grains. Although the $CH_3NH_3PbI_3$ film is full surface coverage in type C (Fig. 5c), the grain sizes are only a few hundred nanometers. The grain sizes and the voids among adjacent grains are relevant to the density of nuclei which grows into grain. When the amount of CH_3NH_3I is low, the density of nuclei is low, resulting in large grain size, while due to the lack of crystal nuclei, many voids between (or in) the grains come up, leading to the poor surface coverage. On the contrary, excessive amount of CH_3NH_3I could bring high density of nuclei and cause small grain size. For type B, the $CH_3NH_3PbI_3$ film has full surface coverage and small surface roughness in type B (Fig. 5b). Meanwhile, the grains as large as 3μm were obtained. Full surface coverage and huge grains indicate the few grain boundaries and then a low density of trap states, which is crucial to the TFTs devices performance.

In order to further verify the crystallization of perovskite $CH_3NH_3PbI_3$ films obtained via vapor-assisted solution process, X-ray diffraction (XRD) measurements were taken. As shown in Fig. 6A. We can see the tiny signature peak at 12.65° is all observed in three types, [36] and the

emergence of a tiny signature peak at 12.65° is relative to the amount of CH_3NH_3I precursor, because PbI_2 could not sufficiently react with CH_3NH_3I, when the amount of CH_3NH_3I precursor was low. However when the amount of CH_3NH_3I precursor was excessive, nuclei of $CH_3NH_3PbI_3$ quickly appeared which resulted high density of nuclei of $CH_3NH_3PbI_3$, then compact $CH_3NH_3PbI_3$ film was obtained on the surface of PbI_2, which hindered PbI_2 further reaction with CH_3NH_3I and resulted in PbI_2 residue. As can be observed (Fig. 6A), type B has almost no PbI_2 residue. At the same time, a representative ultraviolet-visible photoluminescence (PL) spectrum of $CH_3NH_3PbI_3$ thin film (sample B) is shown in Fig. 6B, which consists with previous reports that the PL is right at the band edge. Consequently, it is indicated that the amount of CH_3NH_3I have an obvious influence on crystallization of perovskite $CH_3NH_3PbI_3$ films, then effects perovskite TFT performance.

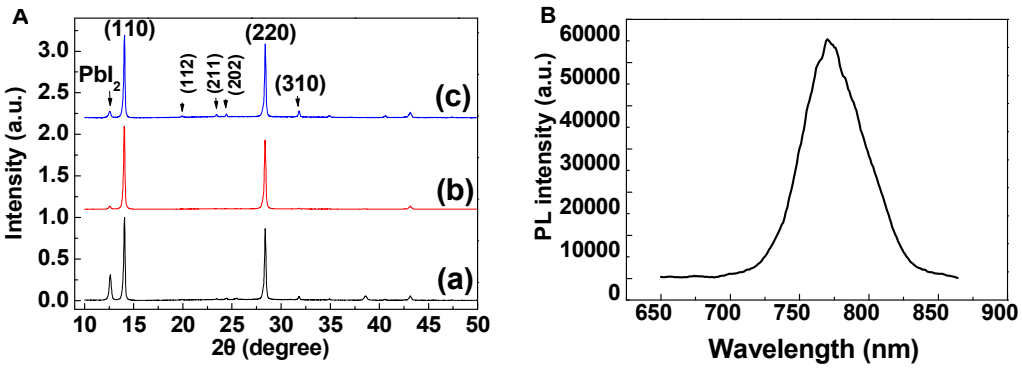

Fig. 6 (A) X-ray diffraction pattern of the $CH_3NH_3PbI_3$ film: the amount of CH_3NH_3I precursor in thermal evaporation process is 120mg (a), 200mg (b), 280mg (c), respectively. (B) A PL spectra for the $CH_3NH_3PbI_3$ thin film of sample B.

3.3 The performances of TFT with $CH_3NH_3PbI_3$ as the channel

Then TFTs with $CH_3NH_3PbI_3$ film as channel layer have been fabricated. This TFTs have a channel length L = 0.5 mm and channel width W = 5 mm, defined by Ag source and drain electrodes. The plot of drain current, I_d, versus gate voltage, V_g, is shown as a function of the

applied same drain voltage V_{ds}= 2V (see Fig. 7a) for TFTs with different types of $CH_3NH_3PbI_3$ channel layer. And obvious electrical field effect is all observed in three types TFTs.

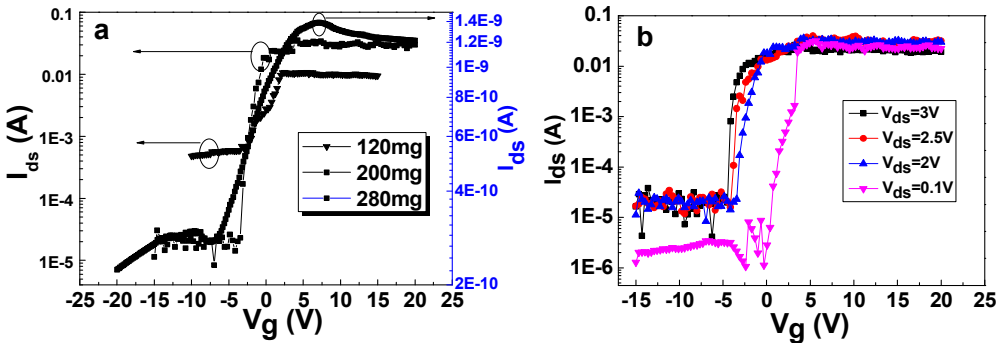

Fig. 7 The plot of drain current I_d versus gate voltage V_g (a) as a function of the amount of CH_3NH_3I precursor for the $CH_3NH_3PbI_3$ film thin-film transistor at V_{ds} = 2 V; (b) as a function of drain voltage V_{ds} for the $CH_3NH_3PbI_3$ film thin-film transistor in type B.

The relevant parameters derived from I_d–V_g measurements corresponding to Fig. 7a are summarized in Table 2. From the plot of I_d versus V_g (Fig. 7a) used to calculate current modulation (I_{ON}/I_{OFF}) and field-effect mobility, μ, in the linear regime. We can see that the performance of TFT in type B is the best, which the field-effect mobility is 566 cm^2/V.s for a ±25 V sweep of V_g at V_{ds} = 2 V with I_{ON}/I_{OFF} >10^4 (Fig. 7a). Simultaneously the sub-threshold current and threshold voltage is the smallest in type B, which value were 0.4035 V/decade, -3.501 V, respectively, which indicates the best device performance (see Table 2) among these three types TFTs. Considering that the un-patterned TFTs show overestimation of field effect mobility due to the peripheral current. Thus, a 30% reduction of the μ should be considered. Additionally, patterning the semiconductor to the active device region also reduces leakage through the insulator contributing to I_{OFF}, increasing I_{ON}/I_{OFF} to at least 10^4. There is no obvious gate induced leakage current in the organic inorganic hybrid perovskite TFTs, which may be related to the special state density distribution of organic inorganic hybrid perovskite materials. This is still under study.

Table 2 Parameters derived from I_d–V_g measurements corresponding to Fig. 7a

$CH_3NH_3PbI_3$ Dosage	I_{ON}/I_{OFF}	Filed-effect Mobility (cm^2/V.s)	Sub-Threshold Current(V/decade)	Threshold Voltage（V）
120mg	22.14	6.41E+01	2.08	-4.47
200mg	2.30E+3	5.66E+02	0.40	-3.50
280mg	6.08	1.02E-02	8.66	-7.83

4. Conclusions

In summary we demonstrated a thin-film field-effect transistor having an organic-inorganic hybrid $CH_3NH_3PbI_3$ material as the semiconducting channel by low-temperature vapor-assisted solution process and made a preliminary optimization of the dosage of the precursors. Finally, we obtained an organic-inorganic hybrid $CH_3NH_3PbI_3$ TFT with field-effect mobility of 396.2 cm^2/V.s, current modulation greater than 10^4, sub-threshold current of 0.4035 V/decade and threshold voltage of -3.501 V. The mobility of organic-inorganic hybrid $CH_3NH_3PbI_3$ TFTs is much higher than that of any other TFTs，such as Si-based TFTs, the metal-oxide TFTs and the best organic TFTs. Meanwhile, this material that can be processed by low temperature, which suggest that organic-inorganic hybrid TFTs may be suitable for applications that require low cost, low temperature, a large area, and the flexibility of plastic substrates. Furthermore, semiconducting organic-inorganic hybrid perovskite materials may be designed with a wide range of organic and inorganic components for use in TFTs and other flexible electronics (for example $CH_3NH_3Pb(I_{1-x}Br_x)_3$). So it is believed that organic-inorganic hybrid perovskite TFTs performance can be further improved by material engineering and optimization of device structure.

Acknowledgements

The work reported here was supported by National Natural Science Foundation of China

(Project No. 61076006), National Natural Science Foundation of China (Zhang; Project No. 61377031) and the Flat-Panel Display Special Project of China's 863 Plan (Project No. 2008AA03A335).

References

[1] S. D. Stranks, G. E. Eperon, G. Grancini, *et al.*, Electron–hole diffusion lengths exceeding 1 micrometer in an organometal trihalide perovskite absorber, *Science*, 2013, **342**(6156), 341–344.

[2] S. R. Forrest. The path to ubiquitous and low-cost organic electronic appliances on plastic. *Nature*, 2004, **428**(6986), 911-918.

[3] G. H. Gelinck, H. E. A. Huitema, E. van Veenendaal, *et al.*, Flexible active-matrix displays and shift registers based on solution-processed organic transistors. *Nature materials*, 2004, **3**(2), 106-110.

[4] A. C. Arias, S. E. Ready, R. Lujan, *et al.*, All jet-printed polymer thin-film transistor active-matrix backplanes. *Applied Physics Letters*, 2004, **85**(15), 3304-3306.

[5] H. Sirringhaus, N. Tessler, R. H. Friend, Integrated optoelectronic devices based on conjugated polymers. *Science*, 1998, **280**(5370), 1741-1744.

[6] L. Zhou, A. Wanga, S.-C. Wu, J. Sun, S. Park, T. N. Jackson. All-organic active matrix flexible display. *Appl. Phys. Lett*. 2006, **88**(8), 3502.

[7] J. W. Jeong, Y. D. Lee, Y. M. Kim, *et al.*, The response characteristics of a gas sensor based on poly-3-hexylithiophene thin-film transistors. *Sensors and Actuators B: Chemical*, 2010, **146**(1), 40-45.

[8] J. Huang, J. Miragliotta, A. Becknell, *et al.*, Hydroxy-terminated organic semiconductor-based

field-effect transistors for phosphonate vapor detection. *Journal of the American Chemical Society*, 2007, **129**(30), 9366-9376.

[9] E. Cantatore, T. Geuns, G. Gelinck, E. van Veenendaal, A Gruijthuijsen, L Schrijnemakers, S Drews, D. De leeuw, A 13.56-MHz RFID system based on organic transponders. *IEEE J. Solid-State Circuits*, 2007, **42**, 84.

[10] K. Myny, S. Steudel, P. Vicca, *et al.*, Plastic circuits and tags for 13.56 MHz radio-frequency communication. *Solid-State Electronics*, 2009, **53**(12), 1220-1226.

[11] C. D. Dimitrakopoulos, D. J. Mascaro, Organic thin-film transistors: A review of recent advances. *IBM Journal of research and development*, 2001, **45**(1), 11-27.

[12] Cheng, Hua-Chi, Chen Chia-Fu, Tsay Chien-Yie. Transparent ZnO thin film transistor fabricated by sol-gel and chemical bath deposition combination method. Applied Physics Letters, 2007, **90**(1), 012113-3.

[13] H J. Snaith, G L. Whiting, B. Sun, et al., Self-Organization of Nanocrystals in Polymer Brushes Application in Heterojunction Photovoltaic Diodes. *Nano Letters*, 2005, **5** (9), 1653-1657.

[14] S T. Meyers, J T. Anderson, C M. Hung, et al., Aqueous Inorganic Inks for Low-Temperature Fabrication of ZnO TFTs. *J. Am. Chem. Soc,* 2008, **130** (51), 17603–17609.

[15] Li, Chensha，Li Yuning，Wu Yiliang，S. Ong Beng， Loutfy, O. Rafik, ZnO field-effect transistors prepared by aqueous solution-growth ZnO crystal thin film. *Journal of Applied Physics,* 2007, **102**(7), 076101-3.

[16] Seung-Yeol Han, Doo-Hyoung Lee, Herman, S. Gregory, Chih-Hung Chang, Inkjet-Printed High Mobility Transparent–Oxide Semiconductors. *Journal of Display Technology,* 2009,

5(12), 520-524.

[17] P K. Nayak，M N. Hedhili，D. Cha, et al., High performance solution-deposited amorphous indium gallium zinc oxide thin film transistors by oxygen plasma treatment. *Appl Phys Lett,* 2012, **100**(20), 1-4.

[18] D.-H. Lee, Y.-J. Chang, G.S. Herman, C.H. Chang, A General Route to Printable High-Mobility Transparent Amorphous Oxide Semiconductors. *Adv. Mater*, 2007, **19**, 843.

[19] Doo-Hyoung Lee, Seung-Yeol Han, S. Gregory, Herman and Chih-hung Chang, Inkjet printed high-mobility indium zinc tin oxide thin film transistors. *Mater. Chem*. 2009, **19**, 3135

[20] Z. Yu, X. Niu, Z. Liu& Q. Pei, Intrinsically stretchable polymer light-emitting devices using carbon nanotube-polymer composite electrodes. *Adv. Mater,* 2011, **23**, 3989–3994.

[21] J. Lianget al., Silver nanowire percolation network soldered with grapheme oxide at room temperature and its application for fully stretchable polymer light-emitting diodes. *ACS Nano,* 2014, **8**, 1590–1600.

[22] J. Zhang, C. Wang & C. Zhou, Rigid/flexible transparent electronics based on separated carbon nanotube thin-film transistors and their application in display electronics. *ACS Nano,* 2012, **6**, 7412–7419

[23] P. H. Lau, et al., Fully printed, high performance carbon nanotube thin-film transistors on flexible substrates. *Nano Lett,* 2013, **13**, 3864–3869.

[24] S. Kim, J. Park, S. Ju, & S. Mohammadi, Fully transparent pixel circuits driven by random network carbon nanotube transistor circuitry. *ACS Nano*, 2010, **4**, 2994–2998.

[25] N. J. Jeon, *et al.*，Compositional engineering of perovskite materials for high performance

solar cells. *Nature*, 2015, **517**(7535), 476-480.

[26] F. Huang, Y. Dkhissi, W. Huang, *et al.*, Gas-assisted preparation of lead iodide perovskite films consisting of a monolayer of single crystalline grains for high efficiency planar solar cells. *Nano energy*, 2014, **10**, 10-18.

[27] A. Goetzberger, C. Hebling, Photovoltaic materials, past, present, future. *Solar energy materials and solar cells*, 2000, **62**(1), 1-19.

[28] M. A. Green, K. Emery, Y. Hishikawa, W. Warta and E. D. Dunlop, Solar cell efficiency tables. *Progress in photovoltaics: research and applications*, 2015, **23**(1), 1-9.

[29] A. Kojima, K. Teshima, Y. Shirai, *et al.*, Organometal halide perovskites as visible-light sensitizers for photovoltaic cells, *J. Am. Chem. Soc.*, 2009, **131**(17), 6050–6051.

[30] M. M. Lee, J. Teuscher, T. Miyasaka, *et al.*, Efficient hybrid solar cells based on meso-superstructured organometal halide perovskites, *Science*, 2012, **338**(6107), 643–647.

[31] J. Wang, M. Qin, H. Tao, *et al.*, Performance enhancement of perovskite solar cells with Mg-doped TiO2 compact film as the hole-blocking layer, *Appl. Phys. Lett.*, 2015, **106**(12), 121104.

[32] J. H. Im, C. R. Lee, J. W. Lee, *et al.*, 6.5% efficient perovskite equantum-dot-sensitized solar cell, *Nanoscale*, 2011, **3**(10), 4088–4093.

[33] Chong Liu, Jiandong Fan,* Xing Zhang, Yanjiao Shen, Lin Yang, and Yaohua Mai*, Hysteretic Behavior upon Light Soaking in Perovskite Solar Cells Prepared via Modified Vapor-Assisted Solution Process. *ACS Appl. Mater & Interfaces*, 2015, **7**, 9066−9071.

[34] C. R. Kagan, D. B. Mitzi, C. D. Dimitrakopoulos. Organic-inorganic hybrid materials as semiconducting channels in thin-film field-effect transistors. *Science*, 1999, 286(5441):

945-947.

[35] V. M. Burlakov, G. E. Eperon, H. J. Snaith, S. J. Chapman, A. Goriely, Controlling coverage of solution cast materials with unfavourable surface interactions, *Appl. Phys. Lett.* 2014, **104**, 091602.

[36] J. M. Ball, M. M. Lee, A. Hey, H. J. Snaith, Low-temperature processed meso-superstructured to thin-film perovskite solar cells, *Energy Environ. Sci.* 2013, **6**, 1739-1743.

[37] G. E. Eperon, V. M. Burlakov, P. Docampo, A. Goriely, H. J. Snaith, Morphological Control for High Performance, Solution‐Processed Planar Heterojunction Perovskite Solar Cells, *Adv. Funct. Mater.* 2014, **24**, 151-157.

[38] M. Era, T. Hattori, T. Taira, T. Tsutsui, Self-organized growth of PbI-based layered perovskite quantum well by dual-source vapor deposition, *Chem. Mater.* 1997, **9**, 8-10.

[39] C. C. Stoumpos, C. D. Malliakas, M. G. Kanatzidis. Semiconducting tin and lead iodide perovskites with organic cations: phase transitions, high mobilities, and near-infrared photoluminescent properties. *Inorganic chemistry*, 2013, **52**(15), 9019-9038.

[40] M. Liu, M. B. Johnston, H. J. Snaith. Efficient planar heterojunction perovskite solar cells by vapour deposition. *Nature*, 2013, **501**(7467), 395-398.

Graphical Abstract

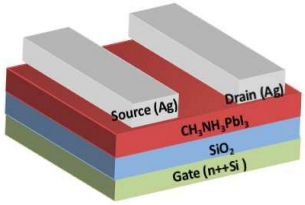

We proposed a new kind of TFT using organic-inorganic hybrid perovskite $CH_3NH_3PbI_3$ material as the semiconducting channel.